7th Workshop on Numerical Methods in Applied
Science and Engineering (NMASE 08)
Vall de Núria, 9 a 11 de enero de 2008

BOUNDS AND ADAPTIVITY FOR 3D LIMIT ANALYSIS

J. Muñoz[1*], J. Bonet[2], A. Huerta[1] and J. Peraire[3]

1: Dep. Applied Mathematics III, LaCàN
Univ. Poitècnica de Catalunya (UPC)
e-mail: j.munoz@upc.edu, web: http://www-lacan.upc.es
2: Civil and Computational Engineering Centre, School of Engineering
University of Wales, Swansea, UK
3: Department of Aeronautics and Astronautics
Massachusetts Institute of Technology, USA

Key words: adaptivity, SOCP, limit analysis, bounds, error estimates

Abstract. *In the present paper we compute upper and lower bounds for limit analysis in two and three dimensions. From the solution of the discretised upper and lower bound problems, and from the optimum displacement rate and stress fields, we compute an error estimate defined at the body elements and at their boundaries, which are applied in an adaptive remeshing strategy. In order to reduce the computational cost in 3D limit analysis, the tightness of the upper bound is relaxed and its computation avoided. Instead, the results of the lower bound are used to estimate elemental and edge errors. The theory has been implemented for Von Mises materials, and applied to two- and three-dimensions examples.*

1 INTRODUCTION

During the last decade, numerical methods for limit analysis have undergone great progress. This is mainly due to the recent development of fast optimisation techniques [Stu99, TTT03], and the increase of the computational capacity, which allow to afford the solution of realistic problems.

The models described in the literature may be mainly characterised by three aspects: (i) the use of strict bounds or estimates of the load factor, (ii) the optimisation techniques used to solve the discretised max-min problem, and (iii) the use of an adaptive remeshing strategy. We will here show two discretisations of the saddle-point problem of limit analysis, one for the bound problem and another for the upper bound problem, which can be solved as a Second Order Cone Program (SOCP). Each one of them yield strict bounds, and yield optimum values of the displacement rate and stress field that are used to design elemental and edge contributions to the bound gap. These values are in turn employed in an adaptive remeshing strategy.

Similar developments have been presented in reference [MBHP] for two-dimensional problems in Von Mises and Mohr-Coulomb plasticity. We extend here the essence of the method to three-dimensional limit analysis with Von Mises plasticity. Although some three-dimensional problems can be found in the literature [LZC04, VaG07, Va07], none of them makes use of adaptive remeshing strategies..

2 STATIC AND KINEMATIC PRINCIPLE

We are interested in finding the collapse load factor λ of a body $\Omega \in \mathbb{R}^{n_{sd}}$ ($n_{sd} = 2, 3$ is the number of space dimensions) subjected to homogeneous Dirichlet and Neumann boundary conditions on $\partial\Omega$, i.e. $\boldsymbol{u} = \boldsymbol{0}$ at Γ_u, and $\boldsymbol{\sigma n} = \lambda \boldsymbol{g}$ at Γ_g, where $\lambda \boldsymbol{u}$ and $\boldsymbol{\sigma}$ are the displacement rate and stress fields, respectively, and $\Gamma_u \cap \Gamma_g = \partial\Omega$. In addition, the load per unit volume $\lambda \boldsymbol{f}$ may be also considered in Ω. We further introduce the linear and bilinear forms:

$$\begin{aligned} a(\boldsymbol{\sigma}, \boldsymbol{u}) &= \int_\Omega \boldsymbol{\sigma} : \boldsymbol{\varepsilon}(\boldsymbol{u}) \, \mathrm{d}V, \\ \ell(\boldsymbol{u}) &= \int_\Omega \boldsymbol{f} \cdot \boldsymbol{u} \, \mathrm{d}V + \int_{\Gamma_g} \boldsymbol{u} \cdot \boldsymbol{g} \, d\Gamma. \end{aligned}$$

where $\boldsymbol{\varepsilon} = \frac{1}{2}(\nabla \boldsymbol{u} + (\nabla \boldsymbol{u})^T)$ is the strain rate. The body is assumed to be a rigid-plastic material, and therfore the stress field is subjected to belong to the set $\mathcal{B}$ of admissible stresses, which in Von Mises plasticity, is given by

$$\mathcal{B} = \{\boldsymbol{\sigma} | dev\boldsymbol{\sigma} : dev\boldsymbol{\sigma} - \frac{2}{3}\sigma_y^2 < 0\}. \tag{1}$$

With this notation and definition at hand, the optimal load factor λ^* is the solution of the following saddle-point problem:

$$\lambda^* = \sup_{\lambda, \boldsymbol{\sigma} \in \mathcal{B}} \inf_{\ell(\boldsymbol{u}) = 1} a(\boldsymbol{\sigma}, \boldsymbol{u}) = \inf_{\ell(\boldsymbol{u}) = 1} \sup_{\boldsymbol{\sigma} \in \mathcal{B}} a(\boldsymbol{\sigma}, \boldsymbol{u}). \tag{2}$$

The first identity gives rise to the static principle of limit analysis, which states that the collapse load factor λ^* corresponds to the maximum external potential that the body can sustain, while being in equilibrium. Indeed, the first identity may be also written as,

$$\begin{aligned} \lambda^* &= \sup_{\lambda, \boldsymbol{\sigma} \in \mathcal{B}} \inf_{\boldsymbol{u}} (a(\boldsymbol{\sigma}, \boldsymbol{u}) - \lambda(\ell(\boldsymbol{u}) - 1)) = \sup_{\boldsymbol{\sigma} \in \mathcal{B}} \inf_{a(\boldsymbol{\sigma}, \boldsymbol{u}) = \lambda \ell(\boldsymbol{u})} \lambda \\ &= \sup \lambda \\ &\quad s.t. \begin{cases} a(\boldsymbol{\sigma}, \boldsymbol{u}) = \lambda \ell(\boldsymbol{u}) \ \forall \boldsymbol{u} \in \mathcal{V} \\ \boldsymbol{\sigma} \in \mathcal{B} \end{cases} \end{aligned} \tag{3}$$

The second identity in (2) gives rise to the kinematic principle, which defining the internal rate of dissipation as $D(\boldsymbol{u}) = \max_{\boldsymbol{\sigma} \in \mathcal{B}} \int_\Omega \boldsymbol{\sigma} : \boldsymbol{\varepsilon}(\boldsymbol{u})$, it states that λ^* is the value of

the minimum $D(\boldsymbol{u})$ subjected to $\ell(\boldsymbol{u}) = 1$. In summary, the optimum values of $(\lambda, \boldsymbol{\sigma}, \boldsymbol{u})$ satisfy the relation $\lambda^* = a(\boldsymbol{\sigma}^*, \boldsymbol{u}^*)$, and due to the saddle-point of structure of the optimum, upper and lower bounds of the load factor, λ^{LB} and λ^{UB}, respectively, may be obtained obtained by satisfying just some of the supremum or infimum in (2), i.e.

$$\lambda^{LB} = a(\boldsymbol{\sigma}, \boldsymbol{u}^*) \leq \lambda^* = a(\boldsymbol{\sigma}^*, \boldsymbol{u}^*) \leq a(\boldsymbol{\sigma}^*, \boldsymbol{u}) = \lambda^{UB}. \tag{4}$$

3 DISCRETISATION AND BOUNDS

We will use discrete spaces $\Sigma^{LB} \times \mathcal{V}^{LB} \ni (\boldsymbol{\sigma}^{LB}, \boldsymbol{u}^{LB})$ and $\Sigma^{UB} \times \mathcal{V}^{UB} \ni (\boldsymbol{\sigma}^{UB}, \boldsymbol{u}^{UB})$ that preserve the first and second inequality in (4), respectively. The choices for such spaces have been specified in Table 1, which are the same used in [Cir04, CPB]. By using them, the optimisation problem in (3) gives rise to the following two discrete problems (see [MBHP, CPB] for their derivation):

$$\lambda^{LB} = \sup \lambda \qquad\qquad \lambda^{UB} = \sup \lambda$$

$$s.t. \begin{cases} \mathbf{A}^{LB}\boldsymbol{\sigma}^{LB} = \mathbf{f}^{LB} \\ \boldsymbol{\sigma}^{LB} \in \mathcal{B}^{UB} \end{cases} \qquad s.t. \begin{cases} \begin{bmatrix} \mathbf{A}^{UB} & \mathbf{B} \end{bmatrix} \begin{Bmatrix} \boldsymbol{\sigma}^{UB} \\ \boldsymbol{t}^{UB} \end{Bmatrix} = \mathbf{f}^{UB} \\ \boldsymbol{\sigma}^{UB} \in \mathcal{B} \\ \boldsymbol{t}^{UB} \in \mathcal{B}_t \end{cases} \tag{5}$$

Bound	Domain	Space	Constrain
UB	Elements	$\boldsymbol{u}^{LB} \in P_0 = \mathcal{V}^{LB}$ $\boldsymbol{\sigma}^{LB} \in P_1 = \Sigma^{LB}$	$div\boldsymbol{u} = 0$ $\boldsymbol{\sigma} \in \mathcal{B}$
	Edges	$\boldsymbol{u}^{LB} \in P_1 = \mathcal{V}^{LB}$	Imposes edge equilibrium
LB	Elements	$\boldsymbol{u}^{UB} \in P_1 = \mathcal{V}^{UB}$ $\boldsymbol{\sigma}^{UB} \in P_0 = \Sigma^{UB}$	$div\boldsymbol{u} = 0$ $\boldsymbol{\sigma} \in \mathcal{B}$
	Edges	$\boldsymbol{t}^{UB} \in P_1$	$\boldsymbol{t} \in \mathcal{B}_t$

Table 1: Spaces used in the upper and lower bound problem for the stress and displacement rate field. No continuity is enforced between elements or edges.

The space $\mathcal{B}_t$ is defined as follows: $\mathcal{B}_t = \{\boldsymbol{t}| \ |\boldsymbol{t}_\tau| \leq \sigma_y/\sqrt{3}\}$, where $\boldsymbol{t}_\tau$ denotes the tangent component of the edge tension. In this way, we ensure that if the stresses at the boundary satisfy $\boldsymbol{\sigma} \in \mathcal{B}$, then $\boldsymbol{t} = \boldsymbol{\sigma}\boldsymbol{n} \in \mathcal{B}_t$.

We remark that the choices in Table 1 preserve the inequalities in (4) [Cir04, CPB, MBHP]. By using $(\Sigma^{LB}, \mathcal{V}^{LB})$, we are satisfying the equilibrium equations of the continuum, and therefore the minimisation is exactly achieved (over the restraint set Σ^{LB}). On the other hand, resorting to spaces $(\Sigma^{UB}, \mathcal{V}^{UB})$ we are able to obtain the maximum

exactly (as a function of the restraint set $\mathcal{V}^{UB}$), or due to the use of a larger projected space $\mathcal{B}_t$, obtain a higher value, and thus an upper bound to λ^* [Cir04, MBHP].

The expressions for matrices $\mathbf{A}^{LB}$,$\mathbf{A}^{UB}$ and $\mathbf{B}^{UB}$, and for vectors $\mathbf{f}^{LB}$ and $\mathbf{f}^{UB}$ have been explicitly given in [MBHP] for two-dimensional cases, but are easily extensible for three dimensions. We will here just comment and give details of the membership constraint of the stresses in (5), in order to turn the optimisation problem in (5) into the form of a SCOP.

For 3D problems, and using the notation $\boldsymbol{\sigma}_{16}^T = (\sigma_1\ \sigma_2\ \sigma_3\ \sigma_4\ \sigma_5\ \sigma_6) =(\ \sigma_{xx}\ \sigma_{yy}\ \sigma_{zz}\ \sigma_{xy}\ \sigma_{xz}\ \sigma_{yz})$, the set $\mathcal{B}$ in (1) is expressed as,

$$\mathcal{B} = \{\boldsymbol{\sigma} | (\sigma_1 - \sigma_2)^2 + (\sigma_1 - \sigma_3)^2 + (\sigma_2 - \sigma_3)^2 + 6(\sigma_4^2 + \sigma_5^2 + \sigma_6) - 2\sigma_y^2 < 0\}.$$

Furthermore, we will use the variables $\boldsymbol{x}_{17}^T =(x_1\ x_2\ x_3\ x_4\ x_5\ x_6\ x_7)$ instead of $\boldsymbol{\sigma}_{16}$. They are both related according to the following transformation:

$$\boldsymbol{x}_{27} = \mathbf{T}^{-1}\boldsymbol{\sigma}_{16} \quad , \quad \boldsymbol{\sigma}_{16} = \mathbf{T}\boldsymbol{x}_{27} \tag{6}$$

with

$$\mathbf{T}^{-1} = \begin{bmatrix} 0 & -\sqrt{6}/2 & \sqrt{6}/2 & 0 & 0 & 0 \\ \sqrt{(}2) & -\sqrt{2}/2 & \sqrt{2}/2 & 0 & 0 & 0 \\ 0 & 0 & 0 & \sqrt{6} & 0 & 0 \\ 0 & 0 & 0 & 0 & \sqrt{6} & 0 \\ 0 & 0 & 0 & 0 & 0 & \sqrt{6} \\ 0 & 1 & 0 & 0 & 0 & 0 \end{bmatrix}, \mathbf{T} = \begin{bmatrix} 1/\sqrt{6} & \sqrt{2}/2 & 0 & 0 & 0 & 1 \\ 0 & 0 & 0 & 0 & 0 & 1 \\ 2/\sqrt{6} & 0 & 0 & 0 & 0 & 1 \\ 0 & 0 & 1/\sqrt{6} & 0 & 0 & 0 \\ 0 & 0 & 0 & 1/\sqrt{6} & 0 & 0 \\ 0 & 0 & 0 & 0 & 1/\sqrt{6} & 0 \end{bmatrix}$$

After using these expressions, it can be verified that the set $\mathcal{B}$ is equivalent to,

$$\mathcal{B} = \{\boldsymbol{x}_{17} | \boldsymbol{x}_{16} \in \mathcal{L}^6, x_7 \text{ free}, x_1 = \sqrt{2}\sigma_y\},$$

where we have introduced the 6th dimensional Lorentz cone $\mathcal{L}^6 = \{\boldsymbol{x} \in \mathbb{R}^6 | x_1 \geq \sqrt{\sum_{i=2}^6 x_i^2}\}$. Similarly, in problem (5)b, the set $\mathcal{B}_t$ is modified by using the variables $\boldsymbol{z}^T = (z_1\ z_2\ z_3)$, and setting $(z_2\ z_3) = \boldsymbol{t}_\tau^T$, which allows to define the admissible set for the boundary tensions as $\mathcal{B}_t = \{\boldsymbol{z} |\ \boldsymbol{z} \in \mathcal{L}^3, z_1 = \sigma_y/\sqrt{3}\}$.

4 ERROR ESTIMATE

The successive refinement of the domain will yield tighter bound gaps $\Delta\lambda = \lambda^{UB} - \lambda^{LB}$. However, the localisation of the displacement rate and tension field jumps that characterises limit analysis, demands the design of effective adaptive remeshing strategies.

In addition, it should be noted that for three-dimensional analysis, the necessary number of elements to obtain tight bounds is considerably higher than in two dimensions. More precisely, for a square domain (cube in 3D) with length L in each dimension, and element size h, the number of elements is given by $nelem_{2D} = 2(L/h)^2$,

while in 3D this is given by $nelem_{3D} = 6(L/h)^3$. In addition, the number of primal variables (stresses) in 2D for the lower bound problem is given approximately by $nvar_{2D} = 3 \times 3 \times nelem_{2D} = 18(L/h)^2$, while in 3D the number of primal nodal variables is $nvar_{3D} = 4 \times 6 \times nelem_{3D} = 144(L/h)^3 = 8(L/h)nvar_{2D}$. Therfore, if uniform remeshing is used, and after 4 remeshing cycles, with similar final ratios L/h, the number of primal variables in 3D analysis is at least 24 times higher than in 2D, which implies a considerable increase of the computational cost. For this reason, adaptive remeshing in 3D analysis is a must. However, while adaptive strategies for 2D problems can be found in [Cir04, CPB, LSKH05, MBHP], adaptive remeshing in 3D is lacking in the literature.

It has been shown in [MBHP] that the total bound gap $\Delta\lambda$ may be expressed as the sum of elemental contributions $\Delta\lambda^e$ and contributions of the edges $\Delta\lambda^\xi$, i.e.,

$$\Delta\lambda = \sum_{e=1}^{nele} \Delta\lambda^e + \sum_{\xi=1}^{N_I} \Delta\lambda^\xi. \tag{7}$$

The elemental and edge contributions are,respectively, given by,

$$\Delta\lambda^e = D^e(\boldsymbol{u}^{UB}) - \underbrace{\left(\int_{\Omega^e} (-\nabla \cdot \boldsymbol{\sigma}^{LB}) \cdot \boldsymbol{u}^{UB} \, \mathrm{d}V + \int_{\partial\Omega^e} (\boldsymbol{n}^e \cdot \boldsymbol{\sigma}^{LB}) \cdot \boldsymbol{u}^{UB} d\Gamma \right)}_{l^e(\boldsymbol{u}^{UB})} \tag{8a}$$

$$\Delta\lambda^\xi = D^\xi(\boldsymbol{u}^{UB}) + \int_{\xi^{e-e'}} \boldsymbol{\sigma}^{LB}\boldsymbol{n} \cdot [\![\boldsymbol{u}^{UB}]\!] \, d\Gamma \tag{8b}$$

where $\boldsymbol{s} = -[\![\boldsymbol{u}^{UB}]\!]/|[\![\boldsymbol{u}^{UB}]\!]|$, and the expression of the elemental plastic dissipation rates $D^e(\boldsymbol{u}^{UB})$ and $D^\xi(\boldsymbol{u}^{UB})$ are given, for Von Mises plasticity, by,

$$\begin{aligned} D^e(\boldsymbol{u}^{UB}) &= \int_{\Omega^e} \sigma_Y \varepsilon_{eq} \, dV \\ D^\xi(\boldsymbol{u}^{UB}) &= \int_{\xi^{e-e'}} \frac{\sigma_Y}{\sqrt{3}} |[\![\boldsymbol{u}^{UB}]\!]| \, d\Gamma. \end{aligned} \tag{9}$$

We remark that due to the use linear edge tension fields, and the numerical integration, the dissipated energy at the edges $D^\xi(\boldsymbol{u}^{UB})$ computed with the optimal values, differs from the analytical expression in (9). The reason for this discrepancy is illustrated in Figure 1 for a one dimensional edge and an hypothetical dissipation energy given by $D(u) = \max_{|t|\leq t_y} \int_\xi tu\mathrm{d}\Gamma$, with t and u scalar tension and displacement rate fields. It can be deduced that in 2D, and using 2 Gauss point quadrature (as it is done in our two-dimensional case), the optimiser will choose the distribution of tensions in Figure b whenever

$$|u_{g1} + u_{g2}| < \frac{u_{g2} - u_{g1}}{\sqrt{3}}.$$

Indeed, the tension field is linear, and functions such as those given in Figure 1b are not. The optimiser will choose a linear function that maximises the integral in the dissipated energy, and thus will provide the optimal tension in Figure 1d. A similar reasoning applies to the two-dimensional edges in 3D problems. Therefore, in order to compute correctly the edge contributions, we have considered the actual values of $|\boldsymbol{t}_\tau^{UB}|$ and not the limit value $\sigma_Y/\sqrt{3}$. We note that in the latter case, a larger error contribution would be obtained, and therefore the equal sign in (7) would become a "$\leq$".

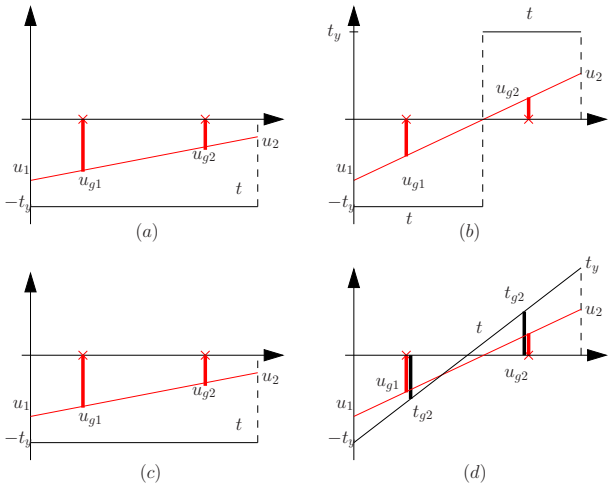

Figure 1: Comparison between analytical values (a,b) and numerical optimal values (c,d) obtained of the tension field t and displacement rates u for a one-dimensional case. Figures (a,c) correspond to a linear field u with no sign variation, and Figures (b,d) a linear field u with a sign variation.

5 UPPER BOUND ESTIMATE

Due to the computational cost of the optimisation problems in (5), we present here a manner to obtain an upper bound without having to actually compute it. Instead of using $\boldsymbol{u}^{UB}$ in expressions (8), we will use the following averaged nodal displacements rates:

$$\bar{\boldsymbol{u}}_n^{UB} = \frac{\sum_{e\ni n}^{n_e} \boldsymbol{u}_{e,n}^{UB}}{n_e} \tag{10}$$

where n_e is the number of elements connected to node n, and $\boldsymbol{u}_{e,n}^{UB}$ is the nodal displacement rate of node n in element e. The upper bound may be then computed as $\bar{\lambda} = \lambda^{LB} + \Delta\lambda(\bar{\boldsymbol{u}}^{UB})$, with $\Delta\lambda$ given in (7). Since we are using a non-optimal displacement rate, the minimisation of the min-max problem is not exactly satisfied, and thus a higher upper bound should be obtained. While this is true for plane stress analysis, where no constrain is solely imposed in the displacement rate field, in the other cases the displacement rate $\bar{\boldsymbol{u}}^{UB}$ will in general not satisfy the constraint given in Table (1), namely $div\boldsymbol{u} = 0$. Consequently, $\bar{\boldsymbol{u}}^{UB}$ is non-optimal and a non-feasible solution of the

dual problem, and hence it cannot be used to compute the error contributions. The numerical experiments in the next section illustrate this fact.

We also note that due to the reasoning described in the previous section, computing the error with the analytical expressions in (9) yields elemental contributions that may be higher than those computed as a SOCP, but in any case will not violate the strictness of the upper the bound.

6 RESULTS

6.1 Vertical cut problem in 2D

We analyise the failure mechanism of a soil subjected to the gravity load and with a vertical cut. The dimensions and the boundary conditions are indicated in Figure 2a. This problem has been already analysed in [LS02a, LS02b, LSKH05, KHS05], and in particular in [MBHP] using the same formulation employed here and the same initial mesh shown in Figure 2. Nonetheless, we present it here to show the effects of averaging the lower bound displacement rates to obtain a non-optimal upper bound solution.

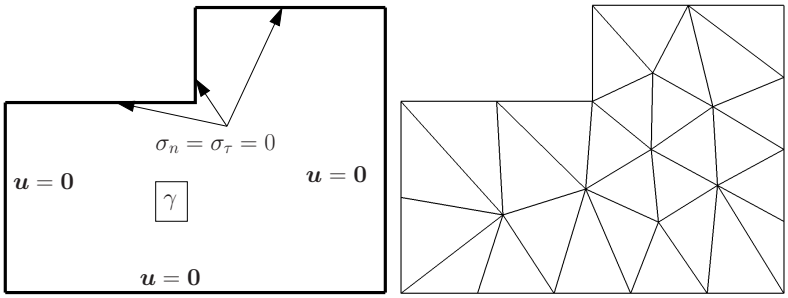

Figure 2: Vertical cut problem geometry and boundary conditions (a), and initial mesh employed (b).

The evolution of the bound gap for plane strain and plane stress is shown in Figure 3, respectively. As mention in Section 5, in plane stress problems, when we average at each node the displacement rates of the lower bound $\boldsymbol{u}^{LB}$, we are obtaining a non-optimal solution, and thus a higher bound than the upper bound computed as a SOCP, λ^{UB}. However, in plane strain, the displacement rate given by $\bar{\boldsymbol{u}}^{UB}$ yield an estimated bound $\bar{\lambda}^{UB}$ which may be higher or lower than λ^{UB}. The bounds in Figure 3 are in agreement with this reasoning. However, it is worth pointing out that in both cases, the resulting error estimate furnishes a lower bound which converges in a similar trend as the lower bound computed with SOCP.

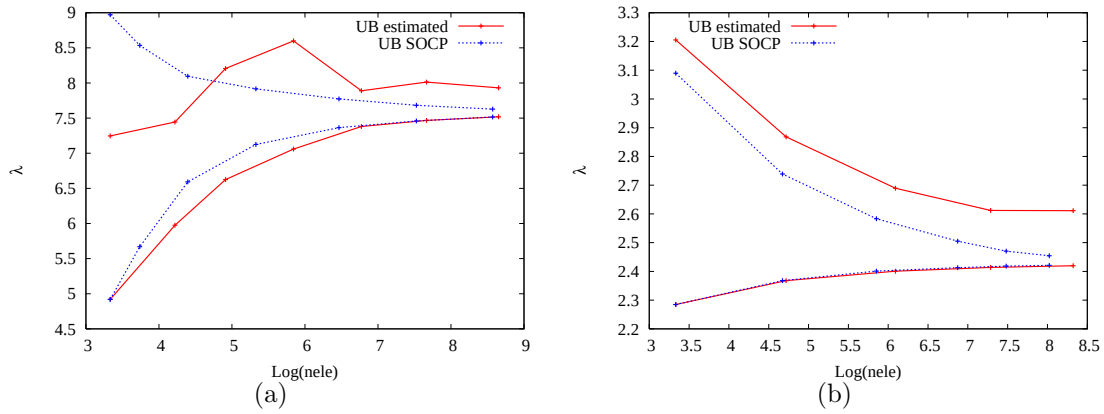

Figure 3: Evolution of the load factor when using computed upper bound with SOCP, and estimated from the lower bound problem for the two-dimensional vertical cut problem in plane strain (a) and plane stress (b).

6.2 Vertical cut in problem in 3D

This a three-dimensional version of the previous problem, and therefore, similar slip lines should be expected. The problem has been run using an initial mesh with 55 elements. Figure 5 shows the deformed mesh after 4 remeshing process, and the values of $|\boldsymbol{t}_\tau|$ at the internal edges. While the deformation pattern is very similar to the two-dimensional case, the evolution of the bounds in Figure 4 reveal a certain lack of convergence of the bounds. However, when using the estimated upper bound according to Section 5, and despite the non-strictness of the upper bound, the lower bound converges. The source of this discrepancy in the two remeshing approaches is currently under investigation.

7 CONCLUSIONS

We have extended the computation of bounds in two-dimensional limit analysis and Von Mises plasticity to three dimensions. We have also extended the error estimates and adaptive remeshing strategy.

While the numerical model is theoretically able to provide such bounds, the numerical tests run so far have revealed the need to reduce the computational cost. More specifically, with the SOCP solvers we have employed [Stu99, TTT03], the bottle neck of the optimisation problem is not as much the time required, but the memory needed to solve practical problems.

In addition, alternative remeshing strategies are being studied to improve the convergence of the bound gap when the upper and lower problems are being solved. research effort is being applied to the reduction paid

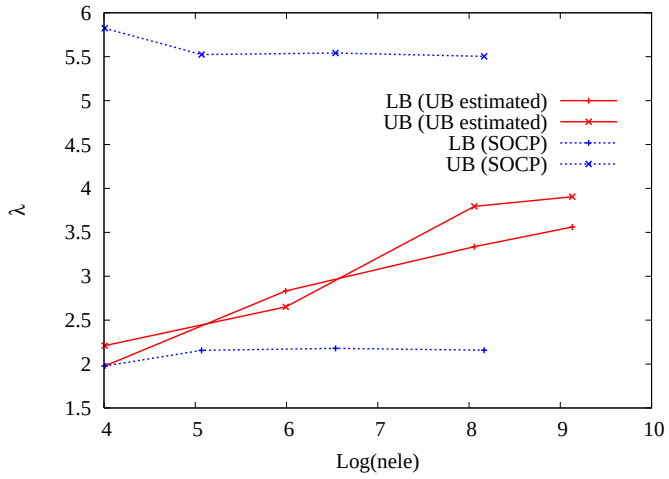

Figure 4: Evolution of the load factor when using computed upper bound with SOCP, and estimated from the lower bound problem for the three-dimensional vertical cut problem.

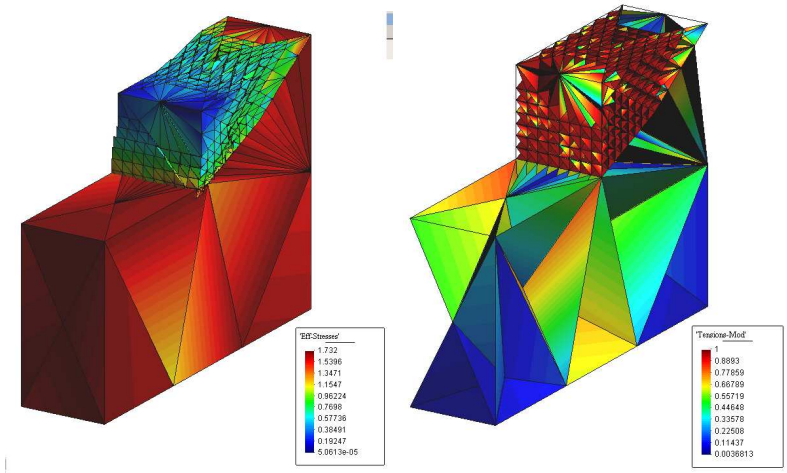

(a) (b)

Figure 5: Effective stresses on the deformed mesh of the upper bound problem (a) and modulus of the tangent edge tensions (b) when using 4316 elements.

REFERENCES

[Cir04] H Ciria. *Computation of Upper and Lower Bounds in Limit State Analysis using Second-Order Cone Programming and Mesh Adaptivity.* PhD thesis, Dep. Aeron. and Astron, MIT, USA, 2004.

[CPB] H Ciria, J Peraire, and J Bonet. Mesh adaptive computation of upper and

lower bounds in limit analysis. *Int. J. Num. Meth. Engng.*. Accepted.

[KHS05] K Krabbenhoft, A V Lyamin M Hjiaj, and S W Sloan. A new discontinuous upper bound limit analysis formulation. *Int. J. Num. Meth. Engng.*, 63:1069–1088, 2005.

[LS02a] A V Lyamin and S W Sloan. Lower bound limit analysis using non-linear programming. *Int. J. Num. Meth. Engng.*, 55:576–611, 2002.

[LS02b] A V Lyamin and S W Sloan. Upper bound limit analysis using linear finite elements and non-linear programming. *Int. J. Num. Anal. Meth. Geomech.*, 26:181–216, 2002.

[LSKH05] A V Lyamin, S W Sloan, C Krabbenhoft, and M Hjiaj. Lower bound limit analysis with adaptive remeshing. *Int. J. Num. Meth. Engng.*, 63:1961–1974, 2005.

[LZC04] Y Liu, X Zhang, and Z Cen. Numerical determination of limit loads for three-dimensional structures using boundary element method. *Eur. J. Mech. A/Solids*, 23:129–138, 2004.

[MBHP] J Muñoz, J Bonet, A Huerta, and J Peraire. Upper and lower bounds in limit analysis: adaptive meshing strategies and discontinuous loading. Submitted.

[Stu99] J F Sturm. Using SeDuMi 1.02, a MATLAB toolbox for optimization over symmetric cones over symmetric cones. *Optim. Meth. Soft.*, 11-12:625–653, 1999. Avail. http://sedumi.mcmaster.ca.

[TTT03] RH Tütüncü, KC Toh, and MJ Todd. Solving semidefinite-quadratic-linear programs using SDPT3. *Mathem. Progr. Ser. B*, 95:189–217, 2003. Avail. http://www.math.nus.edu.sg/ mattohkc/sdpt3.html.

[Va07] M Vicente da Silva and A Ant ao. A non-linear programming method approach for upper bound limit analysis. *Int. J. Num. Meth. Engng.*, 72:1192–1218, 2007.

[VaG07] M Vicente da Silva, A Ant ao, and N Guerra. Numerical implementation of the kinematical theorem: Application to the determination of 3d passive earth pressures of cohesionless. In *COMPLAS2007, Fundamentals and applications*, Barcelona, Spain, 5-7 September 2007. ECCOMAS, Owen et al (eds).

Con el apoyo de *Universitat Politècnica de Catalunya* y *E.T.S. d'Enginyers de Camins, Canals i Ports de Barcelona*